Negative-Valence Neurons in the Larval Zebrafish Pallium

Colton D. Smith[1,2], Zhuowei Du[1,3], William P. Dempsey[1], Scott E. Fraser[1,3,4,5], Thai V. Truong[1,3,4] and Don B. Arnold[1,4,5]

1. Department of Biological Sciences, Division of Molecular and Computational Biology, University of Southern California, Los Angeles, CA 90089
2. Neuroscience Graduate Program, University of Southern California, Los Angeles, CA 90089
3. Translational Imaging Center, University of Southern California, Los Angeles, CA 90089
4. Viterbi School of Engineering, University of Southern California, Los Angeles, CA 90089
5. Department of Quantitative and Computational Biology, University of Southern California, Los Angeles, CA 90089

Abstract:

An organism's survival depends on the rapid classification of sensory events as either harmful or beneficial. In mammals, this computation is partially performed by neurons in the amygdala that respond to signals with negative or positive valence. The larval zebrafish pallium is thought to contain homologs of the mammalian amygdala,

isocortex, and hippocampus; however, the signals encoded by pallial neurons remain largely uncharacterized. Using two-photon light-sheet microscopy to image 7–9-day-old zebrafish that express pan-neuronal GCaMP6s, we recorded calcium dynamics throughout the brain while presenting a panel of strongly aversive stimuli, infrared heat, electric shock, and a whole-field looming shadow, together with milder threats including vibration, loud sound, light transitions, and a partial looming stimulus. A compact cluster of neurons in the rostrolateral dorsal pallium (Rl) responded vigorously to strongly noxious and fully looming stimuli, but not to the milder cues. In contrast, neurons in the ventromedial pallium and habenula responded to all stimuli tested. Rl neurons are characterized by high Tiam2a expression, suggesting they can be genetically accessed. Our results identify a dedicated negative valence locus in the teleost pallium and underscore the evolutionary conservation of valence coding circuits.

Introduction

To evaluate potential threats, organisms must predict future events based on sensory cues (Herberholz and Marquart, 2012). For example, when a predator approaches a fish, sudden changes in water pressure activate its lateral line system, which, combined with visual cues, allows it to predict that danger is imminent and swiftly evade the threat (Olszewski et al., 2012). How fish decide to flee, or, conversely, to mate or feed, remains poorly understood. In mammals, several lines of evidence suggest that this process involves the basolateral amygdala, where distinct ensembles encode negative and positive value (Beyeler et al., 2018; Grewe et al., 2017; Namburi et al., 2015; Tye, 2018; Xiu et al., 2014). Lesions or chemogenetic silencing of the amygdala blunt defensive behaviors and block fear conditioning (Bechara et al., 2003; Corder et al.,

2019; Downer, 1961; Feinstein et al., 2011; LeDoux et al., 1988; Phillips and LeDoux, 1992). The amygdala is also a locus of synaptic change following fear learning (Clem and Huganir, 2010; Goosens and Maren, 2002; Nabavi et al., 2014; Phillips and LeDoux, 1992; Quirk et al., 1995; Rogan et al., 1997). Finally, neurons in the basolateral amygdala project differentially depending on their valence, with negative-valence neurons projecting to the medial central amygdala and neighboring positive-valence neurons projecting to the nucleus accumbens, consistent with activation of the two sets of neurons causing distinct downstream effects (Beyeler et al., 2018; Fadok et al., 2017; Penzo et al., 2014; Tye et al., 2011).

The larval zebrafish (Danio rerio) is an excellent model system for studying sensory processing because its transparent brain is amenable to whole-brain imaging paradigms that require low scattering, such as selective plane illumination microscopy (SPIM; Ahrens et al., 2013). The high speed of SPIM and its low toxicity enable 4-D imaging across large areas of the larval zebrafish brain (Vladimirov et al., 2018). Furthermore, a modified SPIM that uses two-photon excitation (Truong et al., 2011) significantly reduces toxicity and increases penetration relative to 1-P SPIM. Although its brain is smaller and less complex than those of many other vertebrates, the zebrafish can, even in its larval stage, learn to modify responses to environmental stimuli (Gerlai, 2011). In particular, zebrafish are amenable to classical conditioning paradigms, many of which result in activation of distinct regions in the telencephalon (Dempsey et al., 2022; Lal et al., 2018; M Portavella et al., 2004; Portavella et al., 2002; Ruhl et al., 2015). Furthermore, we showed that a well-defined area in the rostrolateral pallium contains

69 neurons that respond to aversive heating (Dempsey et al., 2022). Thus, the rostrolateral
70 pallium of the zebrafish may play similar roles to those of the mammalian amygdala in
71 calculating the valence of sensory stimuli. To test this hypothesis, we investigated
72 whether neurons in the rostrolateral pallium respond specifically to negative-valence
73 stimuli.
74
75 To characterize how neurons in the forebrain of a larval zebrafish respond to sensory
76 stimuli of different valence, we mapped GCaMP (a genetically encoded Ca^{2+} indicator)
77 fluorescence following exposure of the fish to stimuli ranging from highly threatening to
78 mildly aversive. We found a tightly clustered group of neurons in the rostrolateral dorsal
79 pallium that responded vigorously to negative-valence stimuli that are highly predictive
80 of tissue damage, but not to less intense negative-valence stimuli. Two additional areas,
81 the ventromedial pallium and the habenula, contained neurons that responded to both
82 types of stimuli. Negative-valence neurons in the rostrolateral pallium specifically
83 expressed *tiam2a*, a homolog of a gene expressed in the mammalian hippocampus.
84 Thus, we conclude that the rostrolateral pallium is a locus of threat assessment in the
85 larval zebrafish brain containing negative-valence neurons that share a molecular
86 marker with neurons in the mammalian hippocampus.

87 **Results**

88 *Noxious stimuli activate pallial neurons*

89 To investigate how neurons in the forebrain respond to negative-valence stimuli, we
90 created a transgenic zebrafish line, Tg[CAG_{NRSE}::GCaMP6s], expressing GCaMP6s
91 (Chen et al., 2013) driven by the chicken β-Actin CAG promoter (Quitschke et al., 1989)

with an NRSE repressor element (Bergeron et al., 2012) added to diminish expression in non-neuronal cells. Wholemount immunostaining for GCaMP6s and the neuronal marker HuC (elav3) in the forebrain of a 7 dpf Tg[CAG_{NRSE}::GCaMP6s] zebrafish shows almost complete overlap of the two labels, suggesting that virtually all neurons in the zebrafish pallium express GCaMP6s (**Fig. S1**). Note that some skin cells expressed GCaMP6s and were thus excluded from all analyses.

To explore the pallial responses to negative-valence stimuli in real time, we imaged the Tg[CAG_{NRSE}::GCaMP6s] zebrafish using a custom-built two-photon (2P) SPIM (Keomanee-Dizon et al., 2020) (**Fig. S2**). The 2P-SPIM microscope generates a 2P-excitation light sheet using ultrafast near-infrared laser pulses. This microscope combines non-linear excitation for high penetration depth with orthogonal light-sheet illumination for high acquisition speed and low photodamage (Truong et al., 2011). We immobilized 7–9 dpf fish by embedding them in agarose and placing them in a holder immediately adjacent to the SPIM's two objectives (**Fig. S2**).

In our initial studies, we exposed the fish to noxious infrared (IR) heating from a laser positioned over the zebrafish's right eye (**Figs. S2, 1A**), which we previously found elicited a strong escape response consisting of a tail flick (Dempsey et al., 2022). The IR stimulus consisted of a series of five 2-second pulses with 2-minute intervals between. Before, during, and after the stimulus, the SPIM imaged a series of optical sections at 11 depths spanning 60 mm, acquired sequentially every 0.12 seconds, completing a stack every 1.33 seconds. We found that three discrete areas in each

115 hemisphere of the zebrafish forebrain showed an overall increase in fluorescence
116 (ΔF/F, see methods) in response to the IR stimulus (**Fig. 1B**). These areas correspond
117 to the left and right habenula (lHb and rHb), left and right rostrolateral pallium (lRl and
118 rRl), and left and right ventromedial pallium (lVm and rVm) (**Fig. S3**). Time-lapse
119 images of fluorescent signals (with background measured before the stimulus
120 subtracted) show an abrupt increase shortly after the stimulus, with average ΔF/F
121 increasing significantly in each of the six areas (**Fig. 1C-E**, n = 5 fish).
122
123 To characterize the response of pallial and habenular neurons more fully, we exposed
124 the fish to electric shock, another noxious stimulus. We used wires placed
125 approximately 1 mm from the otic vesicles (the ears) to deliver 500 mA of current for
126 400 ms (**Fig. 1F**). All six brain regions that increased activity with IR stimulation also
127 showed a qualitative increase in activity following the electric shock (**Fig. 1G, H**). In
128 addition, the average ΔF/F, measured after electric shock, was significantly higher than
129 measurements before the shock (n = 5 fish**, Fig. 1I, J**). These results show that the Hb,
130 Rl, and Vm areas of the pallium bilaterally respond to two different noxious stimuli.
131
132 To better understand activity at the level of individual neurons, we used the Ca^{2+} signal
133 detection program CaImAn (Giovannucci et al., 2019) to extract neuronal responses
134 from the raw fluorescence data (see methods). Because the CaImAn program cannot
135 reliably distinguish signals from axons, dendrites, and somata, the signals may not
136 represent distinct cells; thus, we refer to the traces produced by CaImAn as "neuronal
137 components". We counted the number of neuronal components with averaged ΔF/F

138 responses that increased by 50% or more compared with before the stimulus, which we
139 refer to as "activated", and those that decreased by 50% or more, which we refer to as
140 "inhibited" (**Fig. 2A, B**). In response to IR heating, the ratio of activated to inhibited
141 neuronal components (A/I) was 5.0 for Hb, 2.0 for RI, and 4.8 for Vm (**Fig. 2C**).
142 Similarly, responses to electric shock had A/I ratios of 2.8 for Hb, 1.8 for RI, and 4.0 for
143 Vm (**Fig. 2D**).
144
145 Although it was not possible to expose the fish to multiple stimuli within a single imaging
146 session due to their fragility, we plotted the cumulative distribution of activated vs.
147 inhibited neuronal components onto a canonical fish template for both IR heating and
148 electric shock so that we could compare responses to the two stimuli (**Fig. 2C, D**). In RI,
149 components activated by both IR heating and electric shock were generally located in
150 the same region, caudal and medial to the region containing inhibited components.
151
152 **Distinct responses to full and partial looming stimuli in RI**
153 Given that two different noxious stimuli evoked activity in Hb, RI, and Vm (**Figs. 1, 2**),
154 we asked how the same regions would respond to a non-noxious stimulus that still
155 indicated an imminent threat of bodily harm. For many visual species, including
156 zebrafish, a looming stimulus consisting of a black disc that increases in size, mimicking
157 the shadow of an approaching predator, signals a potential threat and triggers
158 evolutionarily hard-wired defensive behaviors like freezing or fleeing (Neo et al., 2015).
159 To generate a looming stimulus, we projected a black disc onto a small projector screen
160 located to the right of the 7–9 dpf zebrafish, which started as a 1° point and grew over

161 500 ms to cover the fish's entire visual field. After remaining at full size for 5 s, the disc
162 contracted back to 1°. During this sequence, we monitored GCaMP fluorescence.
163 Similar to exposure to IR heating and electric shock, the full looming stimulus
164 immediately elicited increased activation in all six regions activated by noxious stimuli
165 (**Fig. 3A-C**). There was residual activity in several areas, including rVm, rRl, and lRl 8 s
166 after the stimulus ceased. Quantitation of the average ΔF/F before and after
167 presentations showed significant increases in all six areas (one-way t-test, n = 5, **Fig.**
168 **3D, E**).
169
170 Given the robust response to the full looming stimulus, we asked whether a similar, but
171 less intense stimulus, might elicit a different neuronal response. Thus, we developed a
172 partial looming stimulus, which is similar to the full looming stimulus, except the disc
173 stops growing after 300 ms when it covers approximately 48 degrees of the visual field,
174 and then, after 5 s, reduces in size over 300 ms to a 1° point, which could mimic a
175 predator that comes close to the fish but then stops (**Fig. 3F**). Strikingly, the partial-
176 looming stimulus did not elicit a significant overall ΔF/F increase in Rl, although
177 increases in activity in Hb and Vm were significant (one-way t-test, n = 7, **Fig. 3G-J**).
178
179 A/I ratios of individual activated and inhibited neuronal components responding to the
180 full looming stimulus were 7.2 in Hb, 1.4 in Rl, and 5.5 in Vm, indicating that activation
181 predominated overall (**Fig. 4A**, **C**). However, in response to the partial looming stimulus,
182 neuronal components showed an A/I of 1.2 in Hb and 3.0 in Vm, whereas inhibited
183 components predominated in Rl (A/I = 0.41; **Fig. 4B**, **D**). Thus, multiple measures of

184 neuronal activity are consistent with RI being activated by noxious stimuli and a full
185 looming stimulus, but not by a partial looming stimulus. In contrast, Vm and Hb are
186 activated by all stimuli tested.
187
188 **Mild negative-valence stimuli do not activate RI neurons.**
189 To further test whether RI neurons respond only to highly threatening stimuli, such as
190 noxious stimuli, or to a full looming stimulus, we exposed larval zebrafish to stimuli that
191 could be perceived as threatening but do not indicate imminent bodily harm and
192 measured the response in Hb, RI, and Vm. Specifically, we exposed the zebrafish to
193 sudden vibration, loud noises, and a transition from light to darkness. Each of these
194 stimuli has been shown to elicit startle responses, including C-bends, in larval zebrafish
195 (Beppi et al., 2021; Neo et al., 2015), consistent with their being inherently threatening
196 (Bartoszek et al., 2021). To expose the fish to vibration while recording GCaMP activity
197 with the SPIM, we tapped the right side of the imaging chamber with a plastic stick for 5
198 s. We also presented an auditory stimulus by sounding an airhorn that produced a 120-
199 130 dB sound lasting 0.5 s. Finally, fish that had been equilibrated to darkness, then
200 exposed to light for 4 s, followed by an abrupt return to darkness, were analyzed for
201 response to the light-to-dark transition. Each stimulus was repeated 5 times with a 2-
202 min interval between trials. During and after each stimulus, increased activity was
203 apparent in Hb and Vm, whereas no overall activity change was observed in RI (**Fig**.
204 **5A-I**).
205

206 Statistical analysis showed that overall ΔF/F increased significantly in the rHb, lVm, and
207 rVm in response to tapping, but activity in RI did not increase significantly (one-way t-
208 test, n = 6 fish, **Fig. 6A, B**). Similar results were found for exposure to the air horn blast,
209 where activity significantly increased in Hb and Vm, but not in RI (one-way t-test, n = 4,
210 **Fig. 6C, D**). Finally, overall ΔF/F increased significantly in rHb and lVm, but not in RI,
211 following a dark-to-light transition (one-way t-test, n = 5, **Fig. 6E, F**). Consistent with
212 these results, A/I ratios for the neuronal components found in Hb and Vm ranged from
213 1.6-4.3 but were substantially less than 1 (0.29-0.66) in RI for tapping, airhorn, and light-
214 to-dark transitions (**Fig. 7A-F**). Thus, overall activity in Hb and Vm increases
215 significantly in response to moderately threatening stimuli- at least unilaterally- and
216 activated neuronal components outnumber those that are inhibited. In contrast, in RI,
217 overall ΔF/F does not increase significantly, and inhibited neuronal components
218 outnumber activated ones.
219
220 In conclusion, our results suggest that RI responds exclusively to the most threatening
221 stimuli, but not to less threatening stimuli both in terms of overall activity and A/I ratio of
222 neuronal components (Fig. 8). In contrast, Hb and Vm respond at least unilaterally to all
223 negative-valence stimuli and neuronal components have A/I ratios > 1 (Fig. 8),
224 regardless of whether they are strongly or weakly threatening. Thus, in principle, signals
225 present in RI could be used to identify highly threatening stimuli.
226

227 **Tiam2a-positive neurons in the rostrolateral pallium.**

228 To better understand the properties of neurons in the RI area that respond specifically to
229 imminent threats, we used the MapZebrain cellular-resolution atlas of the larval
230 zebrafish brain (Kunst et al., 2019). We found that in 6 dpf transgenic fish (y264Et, see
231 methods), the Tiam2a promoter drives GFP specifically in a region of the pallium that
232 matches the location of RI neurons. *Tiam2a* is the zebrafish homolog of the mammalian
233 gene *tiam2*, which encodes a Rac1-associated GEF and is expressed primarily in the
234 hippocampus (Chiu et al., 1999).

235

236 To test whether Tiam2a is a marker for neurons that respond to threatening stimuli, we
237 exposed 7–9 dpf Tg[Tiam2a::GFP] larval zebrafish to heating with an IR laser. Then we
238 performed wholemount immunocytochemistry to detect pERK, a marker of neuronal
239 activity. A projection image of GFP and pERK shows striking colocalization between the
240 two markers, with virtually every GFP+ neuron expressing pERK (**Fig. 9A, B**)**.** In
241 contrast, under control conditions with no noxious stimuli present, we observed little
242 pERK expression in GFP+ neurons (**Fig. 9C, D**). To quantify the amount of co-
243 expression between the two, we measured the total intensity of pERK labeling in cells
244 that expressed GFP and subtracted the background intensity of pERK labeling
245 measured in cells in a nearby region of the fish brain that did not express Tiam2a. pERK
246 labeling in GFP+ cells was ~20-fold higher in the IR Laser exposed group (n = 6**)** than in
247 the control group (n = 8), a statistically significant difference (one-way t-test; **Fig 9E**).
248 These data are consistent with Tiam2a being a marker for pallial neurons that are more
249 active when zebrafish are exposed to noxious stimuli.

To investigate the morphology of Rl neurons, we examined Tg[Tiam2a::GFP] fish (**Fig. 9F**). From the dorsal view, GFP-labeled neurons are highly clustered in the rostrolateral pallium, and from the coronal view, they appear superficial and dorsal. Furthermore, they have short axons, suggesting they are involved in local connectivity. Thus, *tiam2a* promoter-mediated expression defines a tightly packed group of neurons that respond to a noxious stimulus in the 7–9 dpf larval zebrafish. These neurons are likely negative-valence neurons that respond specifically to a variety of stimuli, indicating a high likelihood of bodily injury, but not to less threatening aversive stimuli.

Discussion

In this study, we defined responses of neurons in the larval zebrafish forebrain to noxious stimuli (IR heating and electric shock), non-noxious threatening stimuli (full looming), and less threatening stimuli (partial looming, vibration, loud noise, and dark-to-light transitions). Prior research has shown that in the adult zebrafish, neurons in the pallial area Dl, which partially overlaps with Rl, drive ongoing habenular activity (Bartoszek et al., 2021). However, dynamic responses of forebrain neurons to negative-valence stimuli have not been reported previously. Here, we have found that noxious and non-noxious threatening stimuli activate a distinct population of tightly clustered neurons within the rostrolateral dorsal pallium (Rl). However, neurons within this same region do not respond to less threatening stimuli. In contrast, neurons in the ventromedial pallium and the habenula respond to all the stimuli tested, encompassing both highly threatening and mildly aversive stimuli.

In addition to neuronal components activated by negative-valence stimuli, we found components in RI that exhibited reduced activity upon exposure to noxious and threatening stimuli. Previously, it was found that neurons inhibited by negative-valence stimuli may also be activated by positive valence stimuli, suggesting that these neurons may respond to positive valence (Belova et al., 2008; Smith and Torregrossa, 2021). The ratio of activated to inhibited neuronal components was highly correlated with whether the overall signal from a given region increased in response to a specific stimulus. A/I ratio (number of activated vs. inhibited neuronal components) > 1 was correlated with regional activation, whereas A/I < 1 was associated with a lack of activation. In the future, it will be important to test positive-valence stimuli to determine whether they elicit responses in neurons inhibited by negative-valence stimuli. Attempts in this study to elicit a response from forebrain neurons to the smell of food, a positive-valence stimulus, were unsuccessful (data not shown). Additionally, it will be important to determine whether individual neurons in Vm and Hb are broadly tuned to negative-valence stimuli or respond to stimuli of all valences.

It is important to emphasize that RI neurons respond to both looming and noxious stimuli. For cells to be classified as negative-valence, they must respond not only to inherently painful stimuli but also to stimuli that are potentially threatening (Pignatelli & Beyeler, 2018). We found that a full-coverage looming shadow activated rostrolateral neurons, along with ventromedial and habenular regions, in a manner similar to physically noxious stimuli. However, a partial looming shadow failed to elicit a response

296 in RI, although it activated Hb and Vm. Interestingly, it has been shown that when a
297 zebrafish is exposed to a full looming stimulus that covers all of the visual field, it is
298 likely to freeze, whereas a fish exposed to a looming disc that stops growing when the
299 visual field is only partially covered (**Fig. 3F**), is more likely to try to escape (Temizer et
300 al., 2015). Thus, results from this paper suggest that signals from RI- which responds
301 differentially to full and partial looming stimuli- may contribute to the initiation of
302 appropriate defensive behaviors in response to threats.
303
304 In this study, we exploited the unique properties of the larval zebrafish to obtain parallel
305 recordings of neurons throughout the forebrain in response to negative-valence stimuli.
306 One drawback of using larval zebrafish is that they are relatively delicate, making it
307 difficult to present multiple stimuli to the same fish. Consequently, although it is possible
308 to conclude that neurons in RI are likely to respond when the fish is exposed to one of
309 several different stimuli, we cannot conclude that individual neurons respond to more
310 than one stimulus. In addition, it was difficult to relate the stimuli to behavioral
311 responses. Although tail flicks and heart rate were monitored with every response (not
312 shown), there were no uniform responses to specific stimuli. However, electric shock
313 (Kenney et al., 2017; Manuel et al., 2014), looming stimulus (Temizer et al., 2015),
314 vibration (Eaton et al., 2001), loud noise (Eaton et al., 2001; Neo et al., 2015), dark-to-
315 light and light-to-dark transitions (Beppi et al., 2021) all provoked escape behavior when
316 zebrafish were exposed to them in other contexts. It is possible that being encased in
317 agarose, a requirement for SPIM, limited the fish's behavioral responses. In our
318 experiments, and perhaps for agarose-encased zebrafish in other contexts, neural

signatures of negative-valence stimuli are stronger and more consistent than behavioral ones. These findings suggest that forebrain activity, particularly in RI, might be a better indicator of the internal state of the zebrafish's brain than behavior. Together, our results suggest that a transgenic zebrafish expressing GCaMP under the *tiam2a* promoter could provide real-time insight into the animal's internal state.

Several studies have suggested that the dorsomedial pallium in teleost fish, including zebrafish, is the homolog of the amygdala and the dorsolateral pallium is homologous to the hippocampus based on developmental, topological, and molecular arguments (Baker and Wong, 2021; Mueller et al., 2011; von Trotha et al., 2014). In addition, the medial pallium in general and a specific type of pallial neuron were found to be necessary for fear conditioning in zebrafish (Broglio et al., 2005; Lal et al., 2018; Manuel Portavella et al., 2004; Portavella et al., 2002). In contrast, the results from this study and our previous study suggest that rostrolateral neurons are similar in some respects to neurons in the mammalian amygdala. For instance, both of our studies show that rostrolateral neurons respond to negative-valence stimuli, a response also seen in many neurons in the mammalian amygdala (Beyeler et al., 2018). Rostrolateral neurons also become responsive to neutral stimuli following a novel form of classical conditioning (Dempsey et al, 2022). Similarly, following fear conditioning, neurons in the mammalian amygdala become responsive to conditioned stimuli that were paired with unconditioned stimuli (Grewe et al., 2017; Zhang and Li, 2018). Finally, neurons within the rostrolateral region exhibit an increase in excitatory synapses following classical conditioning, and amygdalar neurons undergo long term potentiation, consistent with synaptic change,

following fear conditioning (Rogan et al., 1997). However, unlike the amygdala, where negative- and positive-valence neurons are distributed in a salt and pepper fashion (Beyeler et al., 2018), the negative-valence cells that we found in Rl tend to be tightly clustered (**Fig. 9**). Furthermore, *tiam2a*, is a homolog of mammalian *tiam2*, which is primarily expressed in the hippocampus, and is less abundant in the amygdala (Chiu et al., 1999). Thus, our data suggest that the lateral region of the dorsal pallium shares attributes of both the amygdala and the hippocampus, and that teleost fish may have unique brain structures with no exact homologs in mammals.

Author contributions: C.D.S. and D.B.A. designed the experiments and wrote the paper; C.D.S. performed the live-imaging research, contributed new analytic tools, and analyzed data; Z.D. performed the pERK experiments; T.V.T. and S.E.F. designed and built the SPIM used for live imaging. W.P.D. performed preliminary experiments that were critical for the development of the experimental protocols used in this paper. D.B.A. secured funding and supervised all aspects of the project.

Materials and Methods

Zebrafish husbandry and embryo/larval care

Many of the methods presented in this paper were developed previously (Dempsey et al., 2022). Larval and adult Casper mutant zebrafish were maintained in an in-house veterinary facility in accordance with protocols approved by the University of Southern California (USC) Institutional Animal Care and Use Committee (IACUC). All experiments described in this work were approved by the USC IACUC. Embryos were kept in egg

365 water (1.19 g NaCl, 0.377 g CaSO4·2H2O, 265 mL methylene blue, filled up to 5 liters
366 with ddH_2O) at 28 °C in an incubator with a 13 hr:11 hr light:dark cycle until 5-6 dpf,
367 when they were transferred to tanks within the husbandry facility. On the husbandry
368 system, zebrafish were also maintained on a 13 hr:11 hr light:dark cycle. The air and
369 water temperature in the zebrafish facility are maintained at 26-28°C. Zebrafish larvae
370 used in experiments (7–9 dpf) were transferred between the facility and the
371 experimental apparatus in zebrafish husbandry system water (H.S.W.) and kept at 26-
372 28°C between experiments.
373

374 **Tg[CAG_{NRSE}::GCaMP6s]**

375 To monitor cell Ca^{++} activity in these experiments, we used the transgenic zebrafish
376 Tg[CAG_{NRSE}::GCaMP6s] with GCaMP6s (Chen et al., 2013) expression driven by a β-
377 Actin promoter (Quitschke et al., 1989) to drive widespread expression and 3X NRSE
378 (neuron-restrictive silencer element) to restrict expression to neurons (Bergeron et al.,
379 2012).
380

381 **Tg[Tiam2a::GFP]**

382 The transgenic fish y264Et (originally created by the lab of Harold Burgess), with the
383 construct Et(SCP1:GAL4FF), uniquely labels Tiam2a positive cells with GFP within the
384 rostrolateral pallium (Sprague et al., 2003).

385 This transgenic fish was deposited in the ZFIN database (Ruzicka et al., 2015) with the
386 following citation: Marquart, G.D., Tabor, K.M., Brown, M., Strykowski, J.L., Varshney,
387 G.K., LaFave, M.C., Mueller, T., Burgess, S.H., Higashijima, S., and Burgess, H.A.
388 (2015) Enhancer Trap Transgenics. ZFIN Direct Data Submission. (http://zfin.org).

389 **Mounting Zebrafish in Caddie for Imaging on FlexSPIM**

390 To prepare for behavioral experiments, zebrafish subjects were first embedded in a
391 custom behavioral training caddie generated by Protolabs (Stereolithography, ABS-like
392 Translucent Clear [WaterShed]). Specs: ABS-Like Translucent Clear (WaterShed),
393 Normal Res, Natural, Stereolithography, X: 0.980in Y: 0.206in Z: 0.311in. The caddie is
394 filled with 200 mL of 1% (w/v) agarose, melting point ≤ 65°C (Millipore Sigma;
395 SeaPlaque, Cat:50101) dissolved in egg water containing methylene blue, which
396 suppresses fungal growth. During agarose embedding and fluorescence imaging
397 experiments, zebrafish were anesthetized in a final concentration of 70 ppm MS-222
398 (Western Chemical, Fluka analytical, Cat: A5040-100G) + 70 ppm Isoflurane (Phoenix
399 SKU 012ABB-250CC), an IACUC-approved combination that has been shown to enable
400 fast recovery from anesthesia as compared to using MS-222 alone (Huang WC*, et al.,*
401 2010). The anesthetics are dissolved in filter sterilized HSW. For all experiments
402 involving agarose- embedding of the zebrafish, a 1.5% (w/v) solution of low melting
403 point agarose (Sea Plaque Agarose, Lonza) dissolved in filter sterilized husbandry
404 system water consisting of instant ocean (ASIN: B000255NKA) and baking soda
405 dissolved in reverse osmosis water to achieve pH 7.2 and a conductance of ~700 μS)
406 with anesthetic is used. There was no bias in zebrafish sex for larval experiments, as

407 sex determination does not occur in zebrafish before the juvenile stage, ~24 dpf (Uchida
408 et al., 2002).
409
410 As the agarose solidifies (before it completely solidifies at 5 min), a hair stem (human
411 hair attached to a plastic rod) is used to position the zebrafish so that the body axis is
412 parallel to the surface of the chamber (normal swimming orientation). Once the agarose
413 solidifies, the caddie is placed into a 60 mm culture dish (Corning, Cat: 430166) and 10
414 ml of fresh filter-sterilized H.S.W. is added. The agarose is then shaved down with a
415 razor such that only the head and body are encased. Before the anesthetic wears off
416 after the introduction of the fresh H.S.W. solution (~30 seconds), the tail of the zebrafish
417 (just posterior to the swim bladder) is carefully freed from the agarose using fine forceps
418 (biology tip profile, Fine Science Tools, Cat: 11251-10). The rostral aspect of the
419 zebrafish (anterior to the swim bladder) is held firmly in place by the agarose. The
420 caddie is then transferred to another 60 mm culture dish in preparation for
421 transportation to the imaging room.

422 **FlexSPIM Light Sheet Microscope**

423 After the zebrafish has been mounted into the custom Protolabs caddie, it is ready to be
424 placed onto the flexSPIM. The flexSPIM is a versatile, multi-laser twin-microscope
425 system for light-sheet imaging designed and built for multiphoton and visible wavelength
426 fluorescence light sheet excitation (Keomanee-Dizon et al., 2020). The caddie is
427 securely fastened on the dive bar and placed into the chamber filled with 80 ml of fresh,
428 filter-sterilized H.S.W. During imaging, the objective position is programmed to follow a
429 saw waveform such that the objective takes a unidirectional path starting at the top of

the fish pallium (0 mm) and transitioning through to the most ventral aspect of pallium (60 mm) at a frequency of 0.75 Hz. The brain camera follows a square waveform that instructs it to acquire 11 images per objective cycle.

Arduino

For the behavioral experiments, an Arduino unit (Arduino UNO Rev3, Arduino.cc) and the software (Arduino software [IDE]) from the same company are used to control the stimuli. For the IR experiments, a simple program was designed to control the infrared laser (NIR RLCO-980-1000-F laser, Roithner Lasertechnik) by turning it on and off for two seconds, every two minutes. For the electricity experiments, a simple program was designed to allow the native Arduino 5V output to be turned on and off for 400 ms every two minutes.

Volumetric Visualization of Neural Activation

To visualize stimulus-evoked neural activation, volumetric calcium-imaging data were reconstructed into three-dimensional heat maps. Eleven consecutive image planes acquired with the flexSPIM immediately before stimulus onset were combined to generate a baseline 3D fluorescence volume. The same procedure was repeated for frames acquired after the stimulus (the specific time selected was within a 3 s post-stimulus window to capture the peak GCaMP response). The pre- and post-stimulus volumes were visualized side-by-side to illustrate regional activation patterns. Each 3D volume was rendered in coronal and dorsal orientations and manually curated to exclude superficial skin layers and non-neuronal regions, providing volumetric heat maps of GCaMP fluorescence before and after stimulation

Time-Lapse Analysis of Whole Regions

To quantify the temporal dynamics of stimulus-evoked activity within a region as a whole, time-lapse calcium-imaging data were analyzed from 90 consecutive frames acquired with the flexSPIM, with frame 45 corresponding to stimulus onset. Data from multiple trials were averaged to generate representative activation profiles for the left/right habenula, left/right rostrolateral regions, and left/right ventromedial regions of the brain. Using ImageJ, regions of interest were manually defined, and the mean fluorescence intensity was measured across all frames, producing time-series traces of average neuronal activity before, during, and after each stimulus.

Calcium Imaging Data Processing and Spatial Registration

Time-series calcium-imaging data were processed using the open-source CaImAn package (Giovannucci *et al.*, 2019) to perform motion correction, signal extraction, and neuronal component identification. Rigid and non-rigid motion correction were applied to minimize motion artifacts and ensure accurate spatial alignment across frames. Following registration, a constrained non-negative matrix factorization (CNMF) model was applied, with key input parameters (e.g., expected neuron diameter, local-correlation threshold, and signal-to-noise cut-offs) empirically optimized to match the imaging resolution and fluorescence dynamics of the dataset. This optimization yielded spatial footprints and corresponding $\Delta F/F$ fluorescence traces for individual neuronal components. Model performance was iteratively evaluated through inspection of residual maps and assessment of spatial–temporal consistency.

Neuronal components were selected from anatomically defined regions and depths encompassing the habenula (~10 μm), rostrolateral region (~30 μm), and ventromedial region (~50 μm). Each region consisted of two bilaterally symmetric areas measuring approximately 50 μm × 50 μm. The habenula regions were located at the most caudal aspect of the brain, the rostrolateral regions were positioned rostrally and laterally, and the ventromedial regions were situated ventrally and medially, near the midline of the brain. Within each region, ΔF/F fluorescence traces were extracted for all identified neuronal components.

To correct for gradual fluorescence-intensity drift resulting from photobleaching, a rolling mean filter with a window size of 10 frames was applied to stabilize the ΔF/F time series. For each stimulus type, five trials were performed, except for the partial-looming stimulus, which was presented three times. For every trial, 44 frames preceding (~1min) and 45 frames following (~1min) the stimulus onset were extracted and averaged across trials, with frame 45 corresponding to the time of stimulus delivery. This procedure produced six averaged 90-frame time series per fish, corresponding to left and right hemispheric regions of the habenula, rostrolateral, and ventromedial areas.

To determine which neuronal components exhibited activation or inhibition in response to the stimulus, the mean ΔF/F values from frames 45–50 (post-stimulus window) were compared with the mean of the preceding 40 frames (baseline). Components showing ΔF/F ≥ +50% relative to baseline were classified as activated, while those with ΔF/F ≤ −50% were classified as inhibited.

Binary activation maps, showing activated and inhibited components for all fish and stimulus conditions were then registered onto a canonical template fish (three templates: habenula, rostrolateral, and vetromedial), with activated components represented in red and inhibited components in blue. The canonical template was constructed to represent an "ideal" reference fish and to standardize minor morphological variations across individuals. Registration parameters were manually ascertained using ITK-SNAP, using the midline and the skin-brain boundaries as anatomical landmarks. Using these parameters, each image analyzed was geometrically transformed (cropped, scaled, rotated, and translated) to align with the appropriate canonical template using custom Python scripts incorporating the libraries OpenCV, Matplotlib, and NumPy. The XY coordinates of activated and inhibited components were then extracted from the registered images and plotted onto the canonical template to generate composite activation/inhibition maps showing bilateral regional responses to each stimulus.

Heating Tg[Tiam2a::GFP] Larval Zebrafish using an IR Laser (Figure 9)

Experimental procedures in this section were partially adapted from (Dempsey et al., 2022). To begin, Tg[Tiam2a::GFP] zebrafish larvae were embedded in custom behavioral training molds: a 60 mm culture dish filled with 1% agarose dissolved in egg water, with a 10 mm diameter circle cut out from the center. The zebrafish was anesthetized and then embedded in the 10 mm diameter circle with 500 ml agarose + anesthetic (70 ppm MS-222 + 70 ppm Isoflurane (SKU 012ABB-250CC). While the agarose solidified, the zebrafish's position was parallel to the surface of the chamber, at the top of the agarose surface, and was maintained using a single bristle brush. After 5

518 min, 10 mL of sterilized husbandry system water was added to the chamber. Using fine
519 forceps, the tail of the zebrafish was carefully freed from the agarose. All free-floating
520 agarose was removed from the dish. The dish was then positioned under the objective
521 of a custom-built behavioral microscope such that the right eye of the zebrafish was
522 directly under where the infrared laser spot would be when turned on (NIR RLCO-980-
523 1000-F laser, Roithner Lasertechnik). An Arduino was programmed to deliver the
524 infrared heating laser for two seconds, a total of ten times, with an intertrial separation
525 of 2 minutes. After the fish underwent ten trials, it was then fixed in PFA prior to pERK
526 immunohistochemistry.
527
528 **pERK Immunohistochemistry**
529 After exposing 7–9 dpf Tg[Tiam2a:;GFP] larval zebrafish to the infrared laser ten times,
530 zebrafish were fixed in 4% PFA diluted in 1x PBS (pH 7.4), 70 ppm MS-222, 70 ppm
531 Isoflurane, covered in aluminum foil, and kept at 4°C overnight. Then, fish were washed
532 3 times in 1x PBS (pH 7.4) and 0.25% PBST (0.25% Triton X-100 in PBS). After 3x
533 PBST washes, the zebrafish were placed in 150 mM Tris HCl (pH 9) for 5 min at room
534 temperature, followed by 20 minutes at 65°C. Once this was complete, the samples
535 were cooled to room temperature and given 3x PBST washes. Zebrafish were then
536 permeabilized on ice for 45 minutes with 1x PBS, 0.05% Trypsin-EDTA (Sigma, T4049-
537 100ML) diluted in 1x PBS (pH 7.4). After another 3x PBST wash cycle, the zebrafish
538 were placed for 1 hour at room temperature in blocking buffer solution; (1x PBS, 1%
539 bovine serum albumin, 2% DMSO, 2% NGS, 0.25% Triton X-100. Zebrafish were
540 stained with primary rabbit anti-phosphorylated Erk1/2 antibodies at a 1:300 dilution

541 (Cell Signaling, Catalog #4696) in blocking buffer on a rotating platform at 4°C
542 overnight. After 5X PBST washes, the zebrafish were transferred to a blocking buffer
543 solution containing a 1:1000 dilution of Alexa Fluor 568-conjugated goat anti-rabbit
544 secondary antibody (Invitrogen, A-11011) and incubated overnight at 4°C on an orbital
545 shaker in the dark. After 5 PBST washes, samples were moved to PBS solution and
546 imaged on a Zeiss LSM 780 confocal (Translational Imaging Center, USC).
547

548 **Statistical Analysis**

549 Calcium signal curves and heatmaps were calculated using Python 3.12 scripts.
550 Statistical differences were assessed using paired *t*-tests implemented in the SciPy
551 library, and $p < 0.05$ was considered statistically significant. No statistical methods were
552 used to predetermine sample size.

553 **Experimental Setup and Stimulation Protocols for Neuronal Activity Imaging in**
554 **Fish**

555 All fish used in this study were given 90 min to acclimate on the flexSPIM system.
556 Following acclimation, each fish was imaged for 5 min to establish a baseline for
557 neuronal activity before being exposed to stimuli. The total duration of the experiments
558 was ~15-20 min. After the experiment was finished, the fish was released from the
559 agarose and allowed to rest in a dish for one hour. Only fish that were still alive and
560 healthy after this waiting time were included in the analysis.
561

Near-Infrared laser

Once the fish was prepared for imaging, it was positioned such that its right eye was hit by the IR laser (NIR RLCO-980-1000-F laser, Roithner Lasertechnik). While imaging, the IR laser was turned on for 2 seconds before being turned off. This was repeated 2 minutes later for a total of 5 trials.

Electric shock

Once the fish was prepared for imaging, two 1-pin dual-male jumper wires were secured onto the dive bar such that the pin connectors were positioned on or near both sides of the fish, where the body meets the tail. They were positioned such that when current is applied, it travels between the wires, creating a circuit with the fish in between, causing a small electric shock. While imaging, a 500 mA electric shock was administered to the zebrafish through electrodes connected to a 5 V Arduino pin for 400 ms. This was repeated every 2 minutes, for a total of 5 trials.

Full-looming Stimulus

Once the fish was prepped for imaging, a red-backlit projector screen was positioned on the right side of the fish. The window on the chamber covered 66° of the fish's visual field. A small black circle (1° of the fish's visual field) was maintained throughout the duration of the experiment. At the beginning of each trial, the spot was expanded until it fully covered the entire projection screen (1° to 66 degrees of the visual field) over 500 ms, hence the name "full-looming stimulus". Following 5 s, the stimulus returned to its original size. This was repeated 2 min later for a total of 5 trials.

585 **Partial-looming stimulus**

586 Once the fish was prepped for imaging, it was exposed to a stimulus similar to the full-
587 looming stimulus, except that the black circle expanded to 48° over 300 ms, partially
588 covering the visual field. The black circle remained at 48° for 5 seconds before
589 contracting back to its original size of 1° over 300 ms. This process was repeated 2 min
590 later, for a total of 3 trials.

591

592 **Tapping**

593 During imaging, the experimenter tapped the side of the chamber with a plastic stick for
594 5 s. This process was repeated 2 min later, for a total of 5 trials.

595

596 **Airhorn**

597 While imaging, an air horn (1.4 oz, Betterboat) sounded a 120-130 dB blast
598 approximately 1 inch above the chamber. The experimenter wore ear protection to
599 prevent hearing damage. This procedure was repeated 2 minutes later, for a total of 5
600 trials.

601

602 **Light**

603 Once the fish was prepared for imaging, a red-backlit projector screen was positioned
604 on the right side of the fish, making the light visible to the fish. A small, removable
605 cardboard card was then placed between the fish and the projector, keeping the fish in
606 complete darkness. During imaging, the card was removed for 5 s to expose the fish to

light. After 5 seconds, the card was placed back between the fish and the projector to block the light. This procedure was repeated 2 minutes later, for a total of 5 trials.

Data Availability

Raw and processed data on Jupyter notebooks containing analysis pipelines are available on https://gin.g-node.org/coltonsm/Zebrafish_Valence_Project**.** The DOI for this repository will be made public upon being accepted for publication.

Acknowledgements

We thank M. Jones for microscopy technical support in the Translational Imaging Center, and L. Trinh and E. Carranza Lopez for zebrafish husbandry support. All microscopy was done at the Translational Imaging Center. This work was supported by the National Institute of Mental Health Grant 1UF1NS122082.

References

Ahrens MB, Orger MB, Robson DN, Li JM, Keller PJ. 2013. Whole-brain functional imaging at cellular resolution using light-sheet microscopy. *Nat Methods* **10**:413–420. doi:10.1038/nmeth.2434

Baker MR, Wong RY. 2021. Npas4a expression in the teleost forebrain is associated with stress coping style differences in fear learning. *Sci Rep* **11**. doi:10.1038/s41598-021-91495-7

Bartoszek EM, Ostenrath AM, Jetti SK, Serneels B, Mutlu AK, Chau KTP, Yaksi E. 2021. Ongoing habenular activity is driven by forebrain networks and modulated by olfactory stimuli. *Curr Biol* **31**:3861-3874 e3. doi:10.1016/j.cub.2021.08.021

Bechara A, Damasio H, Damasio AR. 2003. Role of the amygdala in decision-making. *Ann N Y Acad Sci* **985**:356–369. doi:10.1111/j.1749-6632.2003.tb07094.x

633 Belova MA, Paton JJ, Salzman CD. 2008. Moment-to-moment tracking of state value in
634 the amygdala. *Journal of Neuroscience* **28**:10023–10030.
635 doi:10.1523/JNEUROSCI.1400-08.2008
636 Beppi C, Beringer G, Straumann D, Bogli SY. 2021. Light-stimulus intensity modulates
637 startle reflex habituation in larval zebrafish. *Sci Rep* **11**:22410. doi:10.1038/s41598-
638 021-00535-9
639 Bergeron SA, Hannan MC, Codore H, Fero K, Li GH, Moak Z, Yokogawa T, Burgess
640 HA. 2012. Brain selective transgene expression in zebrafish using an NRSE
641 derived motif. *Front Neural Circuits* **6**:110. doi:10.3389/fncir.2012.00110
642 Beyeler A, Chang CJ, Silvestre M, Leveque C, Namburi P, Wildes CP, Tye KM. 2018.
643 Organization of Valence-Encoding and Projection-Defined Neurons in the
644 Basolateral Amygdala. *Cell Rep* **22**:905–918. doi:10.1016/j.celrep.2017.12.097
645 Broglio C, Gomez A, Duran E, Ocana FM, Jimenez-Moya F, Rodriguez F, Salas C.
646 2005. Hallmarks of a common forebrain vertebrate plan: specialized pallial areas
647 for spatial, temporal and emotional memory in actinopterygian fish. *Brain Res Bull*
648 **66**:277–281. doi:10.1016/j.brainresbull.2005.03.021
649 Chen TW, Wardill TJ, Sun Y, Pulver SR, Renninger SL, Baohan A, Schreiter ER, Kerr
650 RA, Orger MB, Jayaraman V, Looger LL, Svoboda K, Kim DS. 2013. Ultrasensitive
651 fluorescent proteins for imaging neuronal activity. *Nature* **499**:295–300.
652 doi:10.1038/nature12354
653 Chiu C-Y, Leng S, Martin KA, Kim E, Gorman S, Duhl DMJ. 1999. Cloning and
654 Characterization of T-Cell Lymphoma Invasion and Metastasis 2 (TIAM2), a Novel
655 Guanine Nucleotide Exchange Factor Related to TIAM1.
656 Clem RL, Huganir RL. 2010. Calcium-permeable AMPA receptor dynamics mediate fear
657 memory erasure. *Science (1979)* **330**:1108–1112. doi:10.1126/science.1195298
658 Corder G, Ahanonu B, Grewe BF, Wang D, Schnitzer MJ, Scherrer G. 2019. An
659 amygdalar neural ensemble that encodes the unpleasantness of pain. *Science*
660 *(1979)* **363**:276–281. doi:10.1126/science.aap8586
661 Dempsey WP, Du Z, Nadtochiy A, Smith CD, Czajkowski K, Andreev A, Robson DN, Li
662 JM, Applebaum S, Truong T V, Kesselman C, Fraser SE, Arnold DB. 2022.
663 Regional synapse gain and loss accompany memory formation in larval zebrafish.
664 *Proc Natl Acad Sci U S A* **119**. doi:10.1073/pnas.2107661119
665 Downer DJLD. 1961. CHANGES IN VISUAL GNOSTIC FUNCTIONS AND
666 EMOTIONAL BEHAVIOUR FOLLOWING UNILATERAL TEMPORAL POLE
667 DAMAGE IN THE "SPLIT-BRAIN" MONKEY, NATURE.
668 Eaton RC, Lee RK, Foreman MB. 2001. The Mauthner cell and other identified neurons
669 of the brainstem escape network of fish. *Prog Neurobiol* **63**:467–485.
670 doi:10.1016/s0301-0082(00)00047-2

671 Fadok JP, Krabbe S, Markovic M, Courtin J, Xu C, Massi L, Botta P, Bylund K, Müller C,
672 Kovacevic A, Tovote P, Lüthi A. 2017. A competitive inhibitory circuit for selection
673 of active and passive fear responses. *Nature* **542**:96–99. doi:10.1038/nature21047
674 Feinstein JS, Adolphs R, Damasio A, Tranel D. 2011. The human amygdala and the
675 induction and experience of fear. *Current Biology* **21**:34–38.
676 doi:10.1016/j.cub.2010.11.042
677 Gerlai R. 2011. Associative Learning in Zebrafish (Danio rerio), Methods in Cell Biology.
678 doi:10.1016/B978-0-12-387036-0.00012-8
679 Giovannucci A, Friedrich J, Gunn P, Kalfon J, Brown BL, Koay SA, Taxidis J, Najafi F,
680 Gauthier JL, Zhou PC, Khakh BS, Tank DW, Chklovskii DB, Pnevmatikakis EA.
681 2019. CaImAn an open source tool for scalable calcium imaging data analysis. *Elife*
682 **8**.
683 Goosens KA, Maren S. 2002. Long-term potentiation as a substrate for memory:
684 evidence from studies of amygdaloid plasticity and Pavlovian fear conditioning.
685 *Hippocampus* **12**:592–599. doi:10.1002/hipo.10099
686 Grewe BF, Grundemann J, Kitch LJ, Lecoq JA, Parker JG, Marshall JD, Larkin MC,
687 Jercog PE, Grenier F, Li JZ, Luthi A, Schnitzer MJ. 2017. Neural ensemble
688 dynamics underlying a long-term associative memory. *Nature* **543**:670–675.
689 doi:10.1038/nature21682
690 Herberholz J, Marquart GD. 2012. Decision Making and Behavioral Choice during
691 Predator Avoidance. *Front Neurosci* **6**:125. doi:10.3389/fnins.2012.00125
692 Kenney JW, Scott IC, Josselyn SA, Frankland PW. 2017. Contextual fear conditioning in
693 zebrafish. *Learn Mem* **24**:516–523. doi:10.1101/lm.045690.117
694 Keomanee-Dizon K, Fraser SE, Truong T V. 2020. A versatile, multi-laser twin-
695 microscope system for light-sheet imaging. *Review of Scientific Instruments* **91**.
696 Kunst M, Laurell E, Mokayes N, Kramer A, Kubo F, Fernandes AM, Forster D, Dal
697 Maschio M, Baier H. 2019. A Cellular-Resolution Atlas of the Larval Zebrafish
698 Brain. *Neuron* **103**:21-38 e5. doi:10.1016/j.neuron.2019.04.034
699 Lal P, Tanabe H, Suster ML, Ailani D, Kotani Y, Muto A, Itoh M, Iwasaki M, Wada H,
700 Yaksi E, Kawakami K. 2018. Identification of a neuronal population in the
701 telencephalon essential for fear conditioning in zebrafish. *BMC Biol* **16**:45.
702 doi:10.1186/s12915-018-0502-y
703 LeDoux JE, Iwata J, Cicchetti P, Reis DJ. 1988. Different projections of the central
704 amygdaloid nucleus mediate autonomic and behavioral correlates of conditioned
705 fear. *J Neurosci* **8**:2517–2529.
706 Manuel R, Gorissen M, Piza Roca C, Zethof J, Van De Vis H, Flik G, Van Den Bos R.
707 2014. Inhibitory avoidance learning in zebrafish (Danio Rerio): Effects of shock
708 intensity and unraveling differences in task performance. *Zebrafish* **11**:341–352.
709 doi:10.1089/zeb.2013.0970

Mueller T, Dong Z, Berberoglu MA, Guo S. 2011. The dorsal pallium in zebrafish, Danio rerio (Cyprinidae, Teleostei). *Brain Res* **1381**:95–105. doi:10.1016/j.brainres.2010.12.089

Nabavi S, Fox R, Proulx CD, Lin JY, Tsien RY, Malinow R. 2014. Engineering a memory with LTD and LTP. *Nature* **511**:348–352. doi:10.1038/nature13294

Namburi P, Beyeler A, Yorozu S, Calhoon GG, Halbert SA, Wichmann R, Holden SS, Mertens KL, Anahtar M, Felix-Ortiz AC, Wickersham IR, Gray JM, Tye KM. 2015. A circuit mechanism for differentiating positive and negative associations. *Nature* **520**:675–678. doi:10.1038/nature14366

Neo YY, Parie L, Bakker F, Snelderwaard P, Tudorache C, Schaaf M, Slabbekoorn H. 2015. Behavioral changes in response to sound exposure and no spatial avoidance of noisy conditions in captive zebrafish. *Front Behav Neurosci* **9**:28. doi:10.3389/fnbeh.2015.00028

Olszewski J, Haehnel M, Taguchi M, Liao JC. 2012. Zebrafish larvae exhibit rheotaxis and can escape a continuous suction source using their lateral line. *PLoS One* **7**. doi:10.1371/journal.pone.0036661

Penzo MA, Robert V, Li B. 2014. Fear conditioning potentiates synaptic transmission onto long-range projection neurons in the lateral subdivision of central amygdala. *Journal of Neuroscience* **34**:2432–2437. doi:10.1523/JNEUROSCI.4166-13.2014

Phillips RG, LeDoux JE. 1992. Differential contribution of amygdala and hippocampus to cued and contextual fear conditioning. *Behav Neurosci* **106**:274–285.

Portavella M, Torres B, Salas C. 2004. Avoidance response in goldfish: emotional and temporal involvement of medial and lateral telencephalic pallium. *J Neurosci* **24**:2335–2342. doi:10.1523/JNEUROSCI.4930-03.2004

Portavella Manuel, Torres B, Salas C. 2004. Avoidance Response in Goldfish: Emotional and Temporal Involvement of Medial and Lateral Telencephalic Pallium. *Journal of Neuroscience* **24**:2335–2342. doi:10.1523/JNEUROSCI.4930-03.2004

Portavella M, Vargas JP, Torres B, Salas C. 2002. The effects of telencephalic pallial lesions on spatial, temporal, and emotional learning in goldfish. *Brain Res Bull* **57**:397–399.

Quirk GJ, Repa C, LeDoux JE. 1995. Fear conditioning enhances short-latency auditory responses of lateral amygdala neurons: parallel recordings in the freely behaving rat. *Neuron* **15**:1029–1039.

Quitschke WW, Lin ZY, DePonti-Zilli L, Paterson BM. 1989. The β actin promoter. *Journal of Biological Chemistry* **264**:9539–9546. doi:10.1016/s0021-9258(18)60565-4

Rogan MT, Staubli U V, LeDoux JE. 1997. Fear conditioning induces associative long-term potentiation in the amygdala. *Nature* **390**:604–607. doi:10.1038/37601

Ruhl T, Moesbauer K, Oellers N, von der Emde G. 2015. The endocannabinoid system and associative learning and memory in zebrafish. *Behavioural Brain Research* **290**:61–69. doi:10.1016/j.bbr.2015.04.046

Ruzicka L, Bradford YM, Frazer K, Howe DG, Paddock H, Ramachandran S, Singer A, Toro S, Van Slyke CE, Eagle AE, Fashena D, Kalita P, Knight J, Mani P, Martin R, Moxon SAT, Pich C, Schaper K, Shao X, Westerfield M. 2015. ZFIN, The zebrafish model organism database: Updates and new directions. *Genesis* **53**:498–509. doi:10.1002/dvg.22868

Smith DM, Torregrossa MM. 2021. Valence encoding in the amygdala influences motivated behavior. *Behavioural Brain Research*. doi:10.1016/j.bbr.2021.113370

Sprague J, Clements D, Conlin T, Edwards P, Frazer K, Schaper K, Segerdell E, Song P, Sprunger B, Westerfield M. 2003. The Zebrafish Information Network (ZFIN): The zebrafish model organism database. *Nucleic Acids Res*. doi:10.1093/nar/gkg027

Temizer I, Donovan JC, Baier H, Semmelhack JL. 2015. A Visual Pathway for Looming-Evoked Escape in Larval Zebrafish. *Curr Biol* **25**:1823–1834. doi:10.1016/j.cub.2015.06.002

Truong T V, Supatto W, Koos DS, Choi JM, Fraser SE. 2011. Deep and fast live imaging with two-photon scanned light-sheet microscopy. *Nat Methods* **8**:757–760. doi:10.1038/nmeth.1652

Tye KM. 2018. Neural Circuit Motifs in Valence Processing. *Neuron*. doi:10.1016/j.neuron.2018.10.001

Tye KM, Prakash R, Kim SY, Fenno LE, Grosenick L, Zarabi H, Thompson KR, Gradinaru V, Ramakrishnan C, Deisseroth K. 2011. Amygdala circuitry mediating reversible and bidirectional control of anxiety. *Nature* **471**:358–362. doi:10.1038/nature09820

Uchida D, Yamashita M, Kitano T, Iguchi T. 2002. Oocyte apoptosis during the transition from ovary-like tissue to testes during sex differentiation of juvenile zebrafish. *J Exp Biol* **205**:711–718.

Vladimirov N, Wang C, Höckendorf B, Pujala A, Tanimoto M, Mu Y, Yang CT, Wittenbach JD, Freeman J, Preibisch S, Koyama M, Keller PJ, Ahrens MB. 2018. Brain-wide circuit interrogation at the cellular level guided by online analysis of neuronal function. *Nat Methods* **15**:1117–1125. doi:10.1038/s41592-018-0221-x

von Trotha JW, Vernier P, Bally-Cuif L. 2014. Emotions and motivated behavior converge on an amygdala-like structure in the zebrafish. *European Journal of Neuroscience* **40**:3302–3315. doi:10.1111/ejn.12692

Xiu J, Zhang Q, Zhou T, Zhou TT, Chen Y, Hu H. 2014. Visualizing an emotional valence map in the limbic forebrain by TAI-FISH. *Nat Neurosci* **17**:1552–1559. doi:10.1038/nn.3813

Zhang X, Li B. 2018. Population coding of valence in the basolateral amygdala. *Nat Commun* **9**. doi:10.1038/s41467-018-07679-9

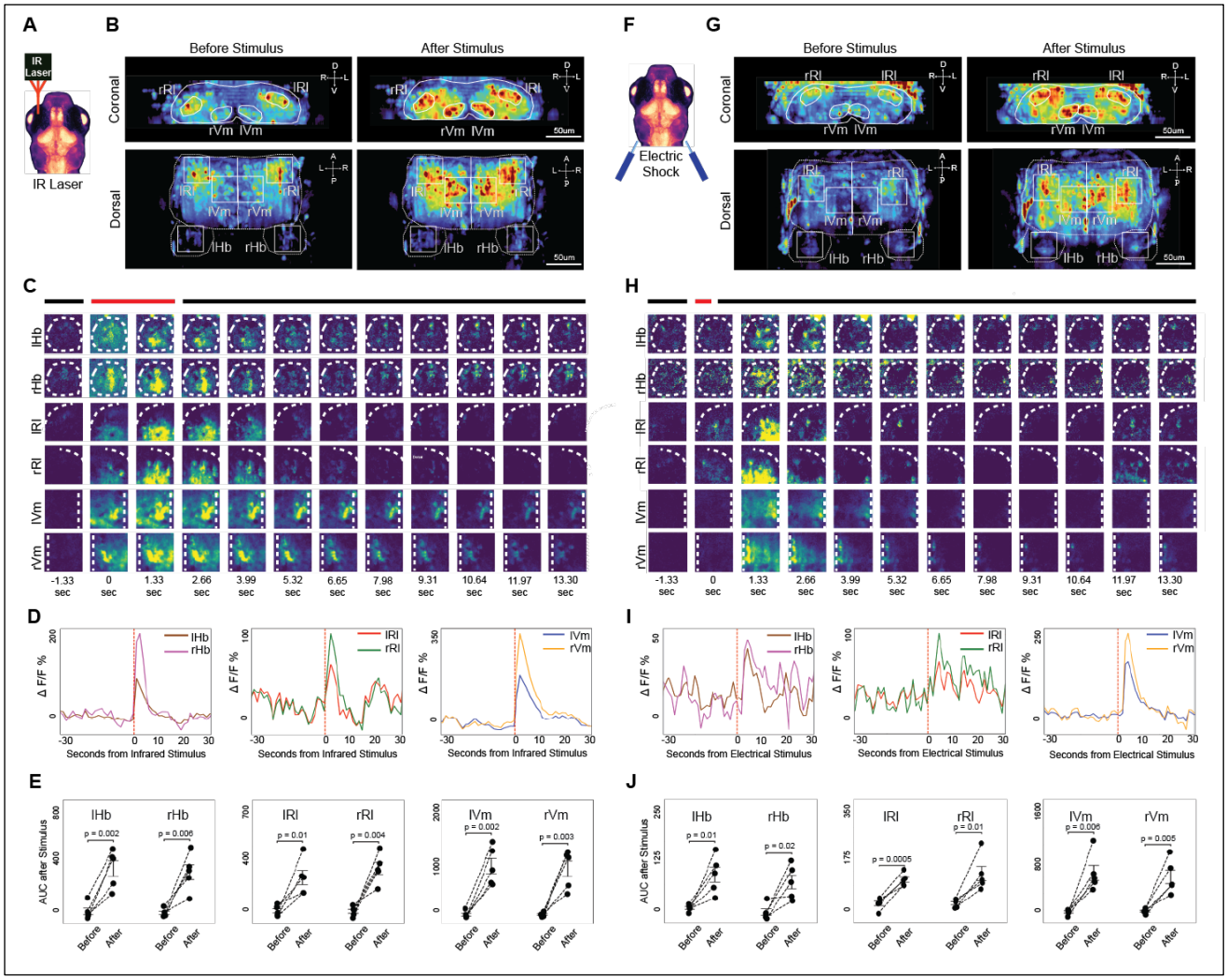

Figure 1 Neuronal activation in response to IR heating and electric shock

(**A**) Experimental setup with an infrared (IR) laser aimed at a 7 dpf larval zebrafish to deliver a heat stimulus.

(**B**) Heat maps of GCaMP fluorescence from a representative fish averaged over 5 presentations of IR heating. Enhanced activity is displayed in rostrolateral (lRL, rRL) and ventromedial (lVm, rVm) areas of the pallium, and habenula (lHb, rHb) in coronal and dorsal views post-laser exposure.

(**C**) Timelapse of average neuronal activation in response to exposure to the IR laser in the forebrain of a representative zebrafish. Each square corresponds to an area outlined in the dorsal view in (B). Brain regions where activity measurements were taken are outlined with dotted lines. Background activity was subtracted from all images.

(**D**) Region-specific ΔF/F activity traces from a representative fish, averaged across 5 trials, display pronounced increases in all measured areas following IR laser exposure.

(**E**) Analysis of the area under the curve (AUC; 5 frames, 6.65 seconds) ΔF/F for each fish for each brain region outlined in (**B**, **C**). Mean ± SEM for n=5 fish.

(**F**) Illustration of electric shock delivery to a 7 dpf larval zebrafish.

(**G**) Heat maps from a representative fish averaged over 5 presentations of electric shock. Enhanced activity is displayed in rostrolateral (lRL, rRL) and ventromedial (lVm, rVm) areas of the pallium, and habenula (lHb, rHb) in coronal and dorsal views post-laser exposure.

(**H**) Timelapse of average neuronal activation in response to exposure to electric shock in the forebrain of a representative zebrafish. Each square corresponds to an area outlined in the dorsal view in (G). Brain regions where activity measurements were taken are outlined with dotted lines. Background activity was subtracted from all images.

(**I**) Region-specific ΔF/F activity traces from a representative fish, averaged across 5 trials, display pronounced increases in all measured areas following electric shock.

(**J**) Analysis of the area under the curve (AUC; 4 frames, 5.32 seconds) ΔF/F for each fish for each brain region outlined in (G, H). Mean ± SEM for n=5 fish.

One-way t-test was used for all statistical comparisons.

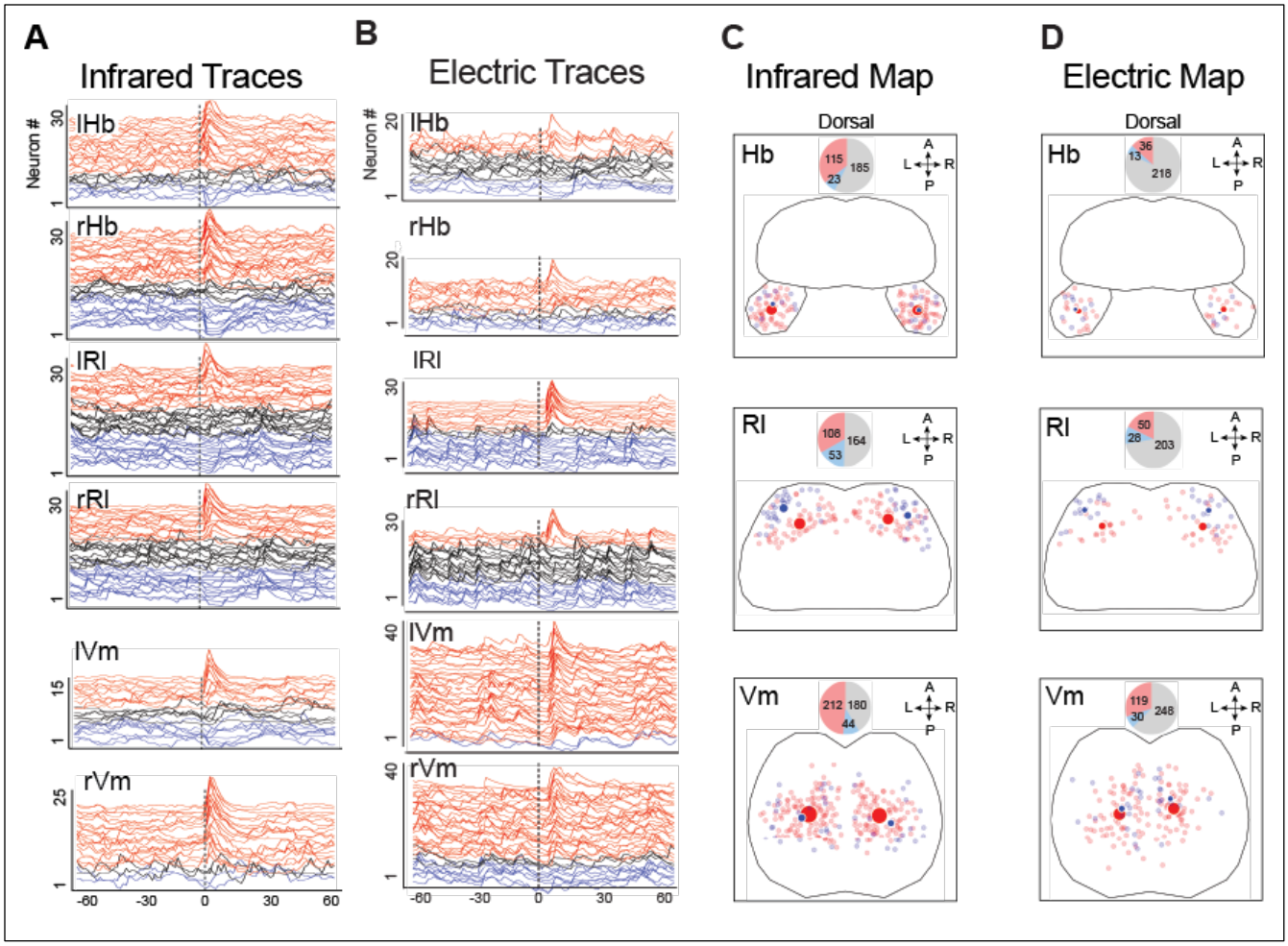

Figure 2. Response of neuronal components to noxious heat stimuli and electric shock.

(A) Neuronal component ΔF/F traces from an example fish as determined by CaImAn reveal a diverse response upon IR stimulation at the vertical dotted line. Red denotes activation (increase in activity ≥ 50% of background DF/F); blue, inhibition (decrease in activity ≤ -50% of background DF/F); Black, neither. Order is determined by z-score (μ/σ), which is a measure of the magnitude and consistency of the response.

(**B**) Neuronal component ΔF/F traces as in (A) in response to electric shock at the vertical dotted line.

(**C**) Locations of activated (small red dots) and inhibited (small blue dots) neuronal components in response to heating with an IR laser for all fish tested. Large dots are centers of mass of corresponding neuronal components. Pie graphs (inset) show the number of activated (red) inhibited (blue), and unresponsive (grey) neuronal components.

(**D**) Same as (C), but for neurons that respond to electric shock

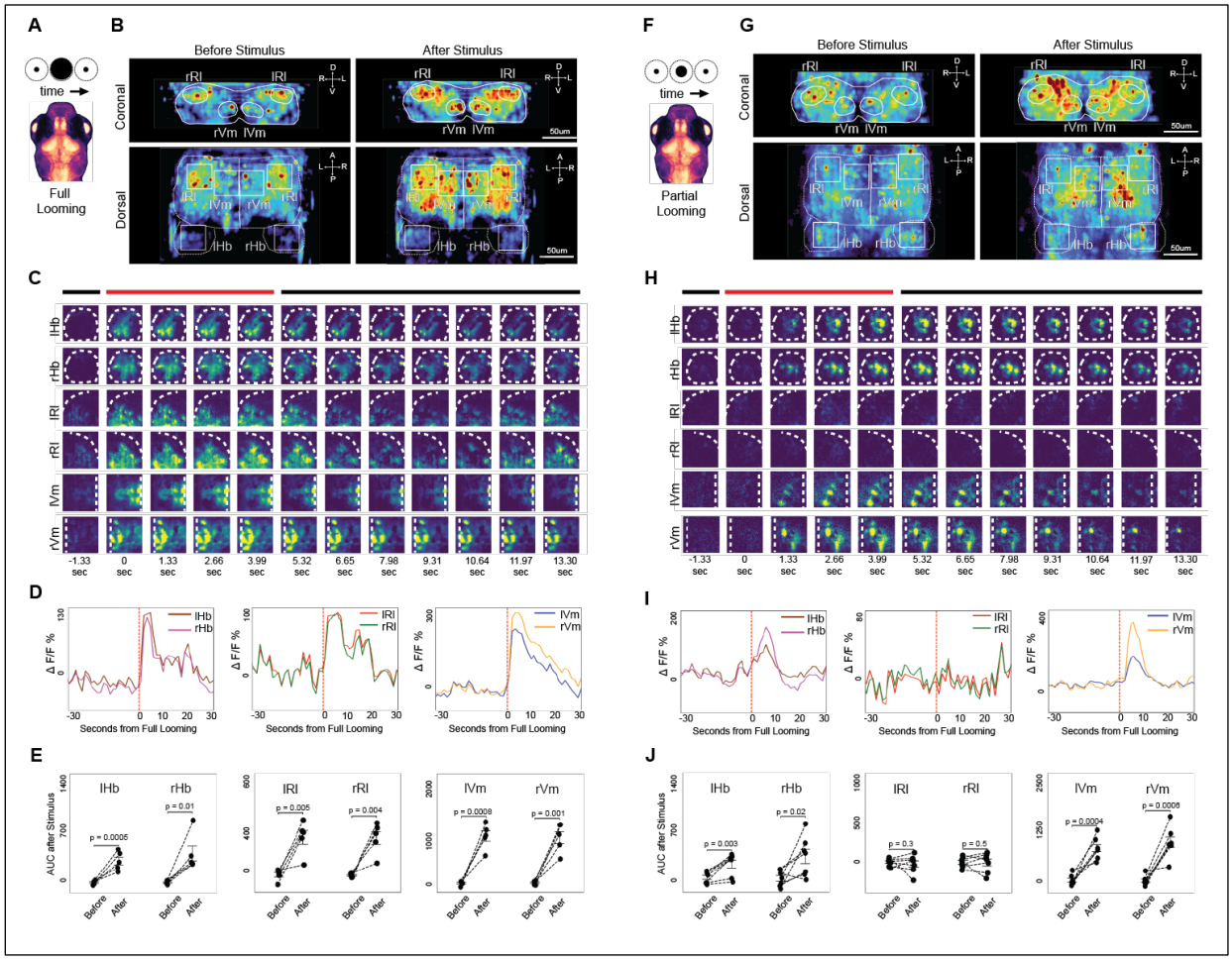

Figure 3. Neuronal activation in response to full and partial looming stimuli.

(**A**) Schematic of a 7 dpf zebrafish subjected to a full-looming disc stimulus.

(**B**) Neuronal activation in a representative zebrafish immediately before and after a full looming stimulus, averaged over 5 presentations, shows an increase in average activity across all brain areas previously found to be activated by noxious stimuli (rHb, lHb, rRl, lRl, rVm, lVm).

(**C**) Timelapse of heatmaps for the six areas outlined in (B) shows an abrupt increase in activity that commences with the full-looming stimulus.

(**D**) Region-specific ΔF/F activity traces from a representative fish, averaged across 5 trials, display pronounced increases in all measured areas following IR laser exposure.

(**E**) Mean increase above background ± SEM for ΔF/F A.U.C. for 5 frames, 6.65 seconds for each fish for each brain region outlined in (B)

(**F**) Schematic of a 7 dpf zebrafish subjected to a partial-looming disc stimulus.

(**G**) Neuronal activation in a representative zebrafish immediately before and after a partial looming stimulus, averaged over 3 presentations.

(**H**) Time-lapse of heatmaps for the six areas outlined in (B) shows an increase in activity in the Hb and Vm regions, but no significant change in activity in the Rl region. Activity in Hb and Vm was sustained for over 10 seconds.

(**I**) Region-specific ΔF/F and activity traces from a representative fish, averaged across 3 trials, display significant activity increases in Hb and Vm, but not in Rl, in response to the partial looming stimulus.

(**J**) Mean increase above background ± SEM for ΔF/F after the partial-looming stimulus (12 frames, ~16 seconds).

All statistical comparisons made with one-way t-test.

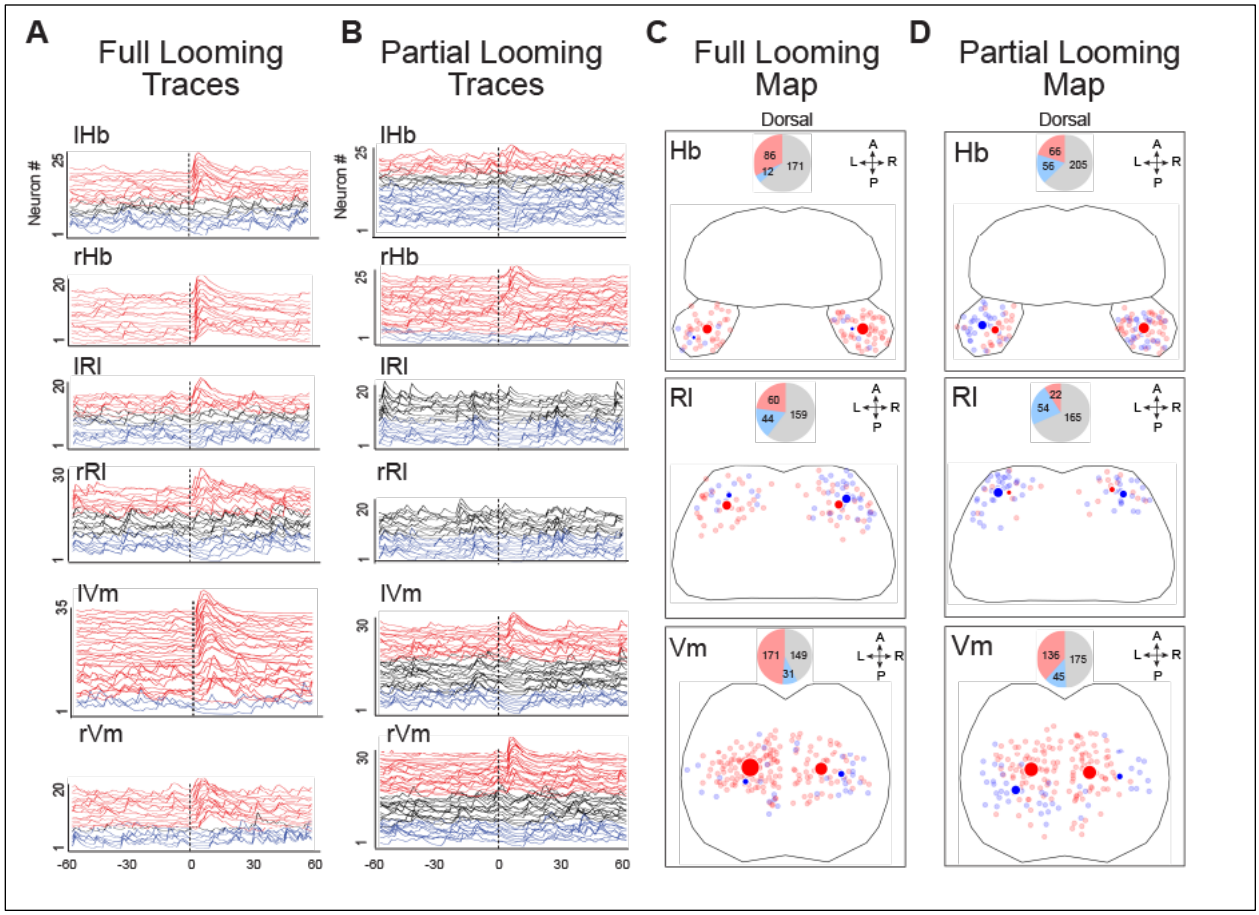

Figure 4. Response of neuronal components to full and partial looming stimuli.

(**A**) Neuronal component ΔF/F traces for an exemplary fish in response to a full looming stimulus at the vertical dotted line, averaged over 5 presentations. Red denotes activation (increase in activity ≥ 50% of background ΔF/F); blue, inhibition (decrease in activity ≤ -50% of background ΔF/F); black, neither. Order is determined by z-score (μ/σ), which is a measure of the magnitude and consistency of the response.

(**B**) Neuronal activity as in (A) in response to a partial looming stimulus averaged over 3 presentations in an exemplary fish. Activated and inhibited traces are seen in Hb and Vm, but not in Rl.

(**C**) Locations of neurons that are activated (small red dots) and inhibited (small blue dots) in response to a full looming stimulus for all fish tested. Large dots are centers of mass of corresponding neuronal components. Pie graphs (inset) show the number of activated (red), inhibited (blue), and unresponsive (grey) neuronal components.

(**D**) Same as (C) in response to a partial looming stimulus for all fish tested.

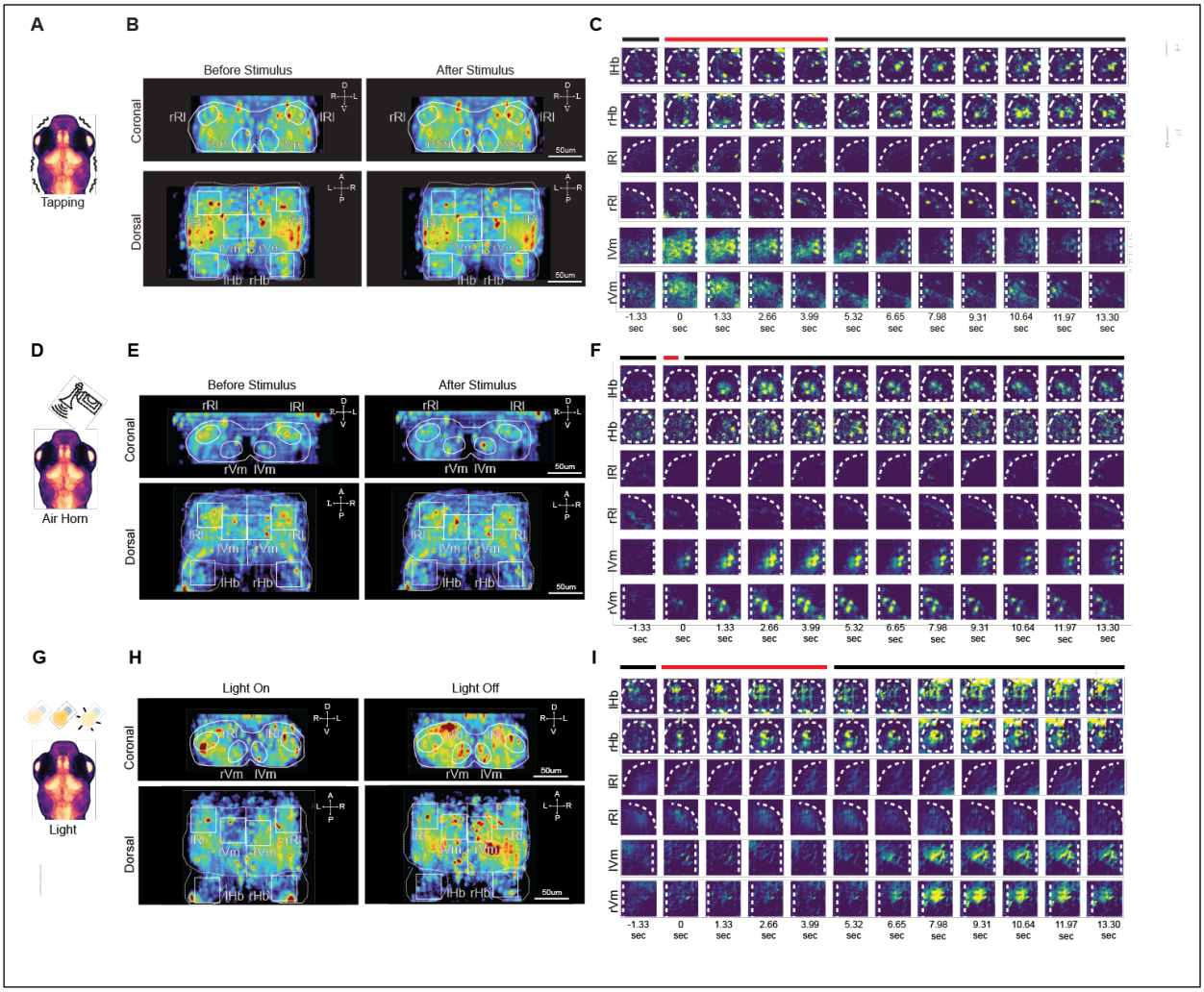

Figure 5. Neuronal activation in response to vibration, a loud noise, and light.

(**A**) Schematic of a 7 dpf zebrafish subjected to vibration.

(**B**) Neuronal activation in a representative zebrafish immediately before and after a vibration stimulus, averaged over 5 presentations, shows an increase in average activity across Hb and Vm, but not RI.

(**C**) Timelapse of heatmaps for areas outlined in (B) show an increase in activity that commences with the initiation of tapping and grows until 14 s after cessation of tapping in Hb. In Vm the activity increases during the tapping stimulus and decreases abruptly after cessation. There is no increase in activity in RI.

(**D**) Schematic of a 7 dpf zebrafish subjected to the blast of an air horn.

(**E**) Neuronal activation in a representative zebrafish immediately before and after an air horn blast, averaged over 5 presentations, shows an increase in average activity across Hb and Vm, but not RI.

(**F**) Timelapse of heatmaps for areas outlined in (E) show an increase in activity that commences with the onset of the loud noise in Hb and Vm and lasts for over 10 s. There is no increase in activity in RI.

(**G**) Schematic of a 7 dpf zebrafish that is first equilibrated to darkness, then exposed to light for 4 s and then returned to darkness.

(**H**) Neuronal activation in a representative zebrafish immediately before and after transitioning from light to darkness, averaged over 5 presentations shows an increase in average activity across Hb and Vm, but not RI.

(**I**) Timelapse of heatmaps for areas outlined in (H) shows an increase in activity in Hb and Vm that commences ~ 2 s after the onset of darkness and lasts for over 5 s. There is no increase in activity in RI.

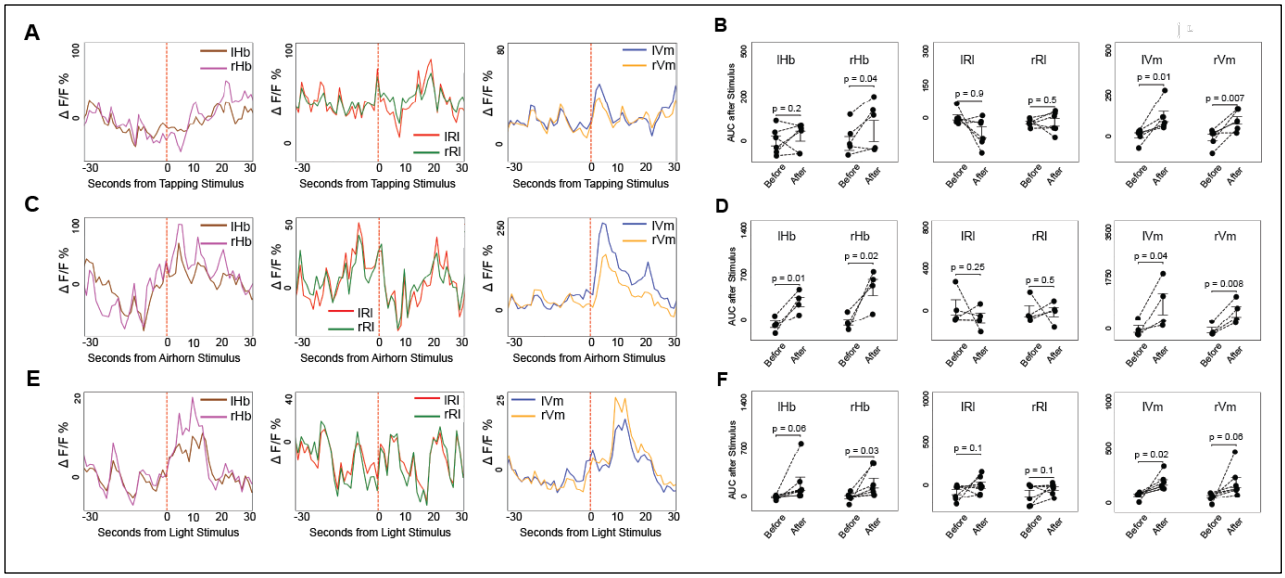

Figure 6 Response of total ΔF/F within different regions to vibration, a loud noise, and light

(**A**) Average ΔF/F activity traces within specific regions from a representative fish, averaged across 5 trials in response to a tapping stimulus.

(**B**) Activity rates for 6 fish before and after the tapping stimulus. Significant increases in activity were seen in rHb, lVm, and rVm, but not in lHb and Rl.

(**C**) Average ΔF/F activity traces within specific regions (AUC; 7 frames, 9.31 seconds) from a representative fish, averaged across 5 trials in response to a blast from an airhorn.

(**D**) Responses to a blast from an airhorn from 4 fish. Significant increases in activity were seen in HB and Vm, but not in Rl.

(**E**) Average ΔF/F activity traces within specific regions from a representative fish, averaged across 5 trials in response to a light-to-dark transition.

(**F**) Responses to a light-to-dark transition from 6 fish. Significant increases in activity were seen in rHB and lVm, but not in lHb, rVm, and Rl.

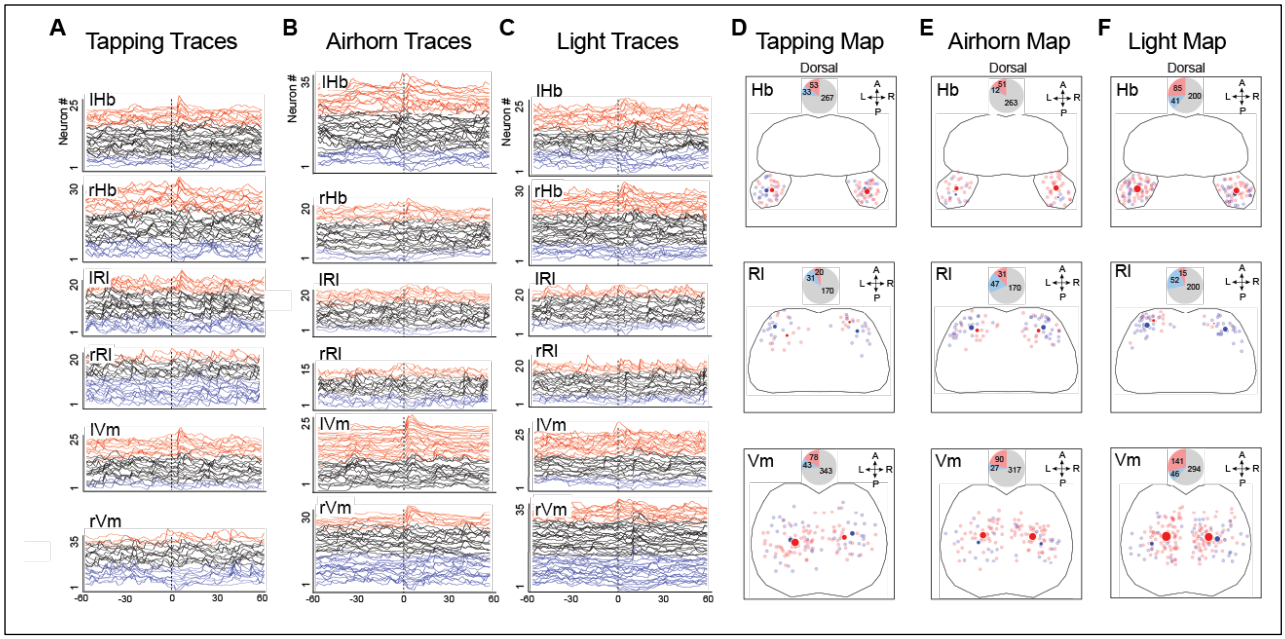

Figure 7 Response of neuronal components to vibration, a loud noise, and light

(**A**) Neuronal component ΔF/F traces of a representative fish in response to tapping at the vertical dotted line. Red denotes activation (increase in activity ≥ 50% of background ΔF/F); blue, inhibition (decrease in activity ≤ -50% of background ΔF/F); black, neither. Order is determined by z-score (μ/σ), which measures the magnitude and consistency of the response. In Hb and Vm, the responses of neuronal components to all three stimuli tend to be better defined than those in RI.

(**B, C**) Neuronal component ΔF/F traces as in (A), but in response to the blast of an airhorn (B) or a transition from light to dark (C) at the vertical dotted line.

(**D-F**) Locations of neuronal components in Hb, RI, and Vm. Small puncta mark locations where neuronal components respond by increasing (red) or decreasing (blue) activity in response to tapping (D), a blast from an airhorn (E) or a transition from light to dark (F). Large dots represent centers of mass of corresponding neuronal components. Pie graphs (inset) show the number of activated (red), inhibited (blue), and unresponsive (grey) neuronal components. Note that in RI, inhibited neurons dramatically outnumber activated neurons, whereas in Hb and Vm, the proportion of activated components are roughly equal to or greater than that of inhibited components.

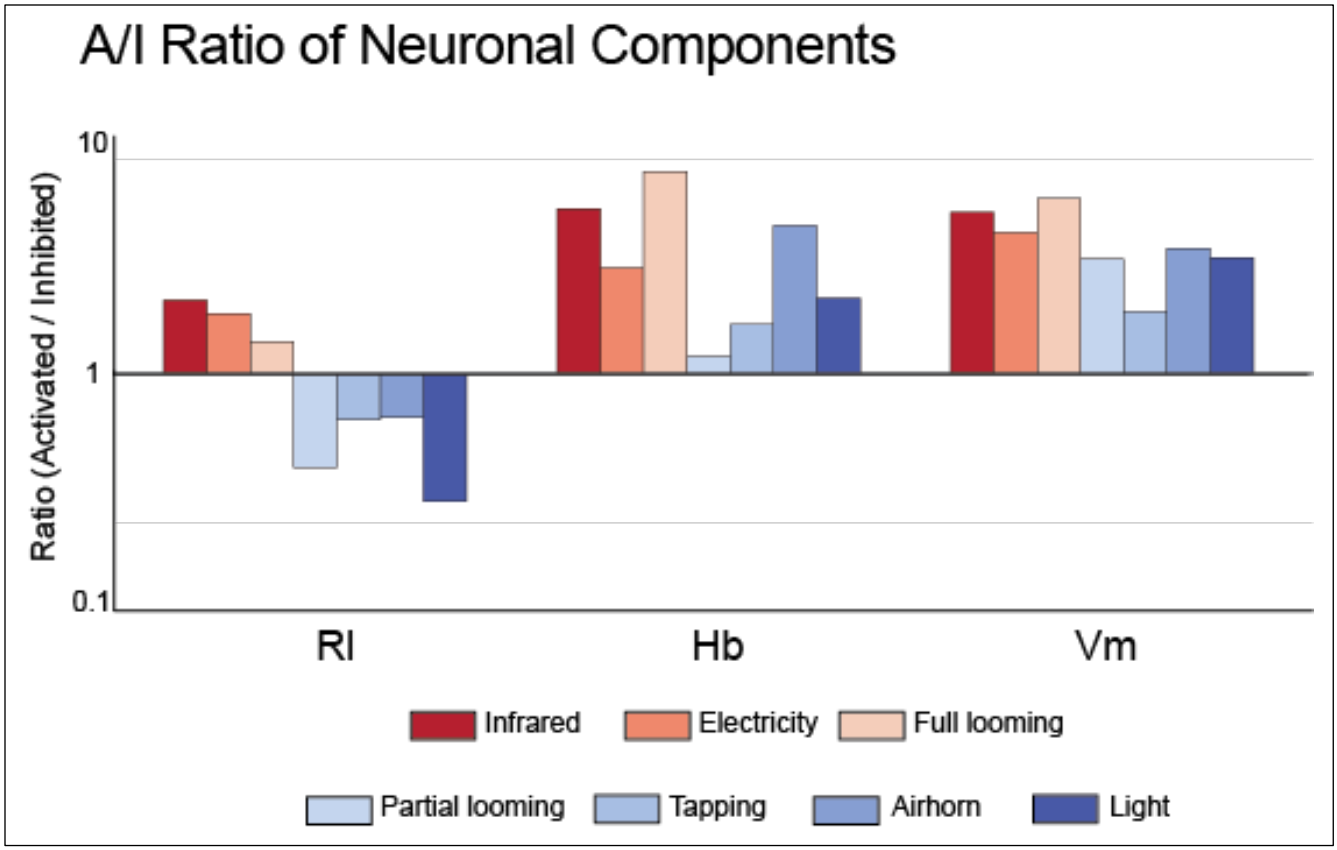

Figure 8 RI is activated by highly threatening stimuli but not by mildly threatening stimuli.

The ratio of activated to inhibited neuronal components (A/I) in RI is greater than 1 for highly threatening stimuli but less than 1 for mildly aversive stimuli. In contrast, in Hb and Vm, the A/I ration is greater than one for all aversive stimuli.

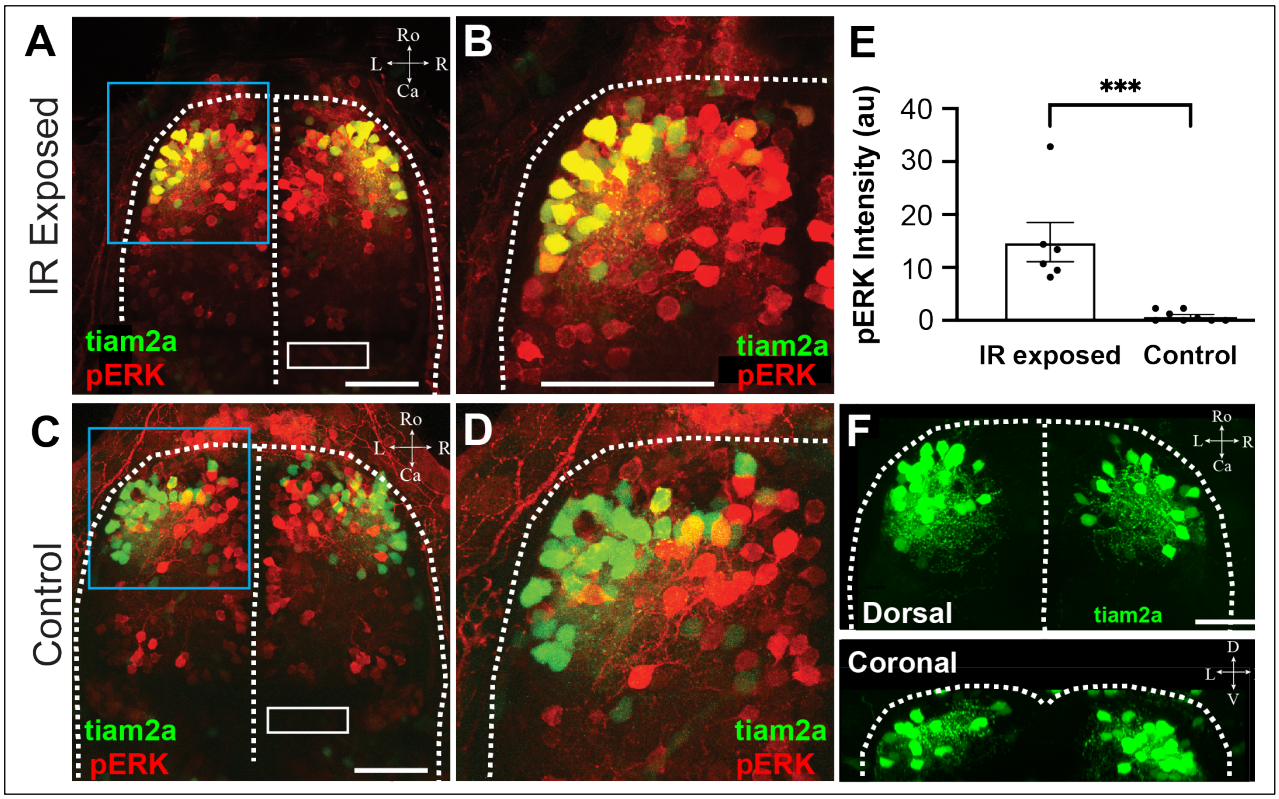

Figure 9 Cells expressing tiam2a become active when exposed to IR heating.

(**A**) 7 dpf Tg[Tiam2a::GFP] larval zebrafish exposed 10 times to heating with an IR laser and then immunostained for pERK to label active neurons. Virtually all GFP-positive neurons were co-labeled with pERK, suggesting that Tiam2a-positive cells are activated by a painful stimulus.

(**B**) Close-up of the area bordered by the blue rectangle in (A).

(**C**) 7 dpf Tg[Tiam2a::GFP] larval zebrafish control that was not exposed to heating showed very little overlap between GFP labeling and labeling for pERK.

(**D**) Closeup of the area bordered by the blue rectangle in (C).

(**E**) Average intensity of pERK immunostaining in Tiam2a+ cells, with background (measured in the white rectangle in (A)) subtracted, for fish exposed to IR heating (n = 6) and control fish (n = 8). Significantly more labeling was found in fish exposed to heating (P = 0.0009, t-test) vs. in control fish.

(**F**) Tg[Tiam2a::GFP] fish showing cell bodies concentrated in the rostrolateral area and local axonal connections.